hnRNP R and its main interactor, the noncoding RNA 7SK, coregulate the axonal transcriptome of motoneurons

Michael Briese[a,1], Lena Saal-Bauernschubert[a,1], Changhe Ji[a,1], Mehri Moradi[a], Hanaa Ghanawi[a], Michael Uhl[b,c], Silke Appenzeller[d,e], Rolf Backofen[b,c], and Michael Sendtner[a,2]

[a]Institute for Clinical Neurobiology, University of Wuerzburg, 97078 Wuerzburg, Germany; [b]Department of Computer Science, Albert-Ludwigs-Universität Freiburg, 79110 Freiburg, Germany; [c]Centre for Biological Signalling Studies, Albert-Ludwigs-Universität Freiburg, 79104 Freiburg, Germany; [d]Core Unit Systems Medicine, University of Wuerzburg, 97078 Wuerzburg, Germany; and [e]Comprehensive Cancer Center Mainfranken, University of Wuerzburg, 97080 Wuerzburg, Germany

Edited by Don W. Cleveland, University of California, San Diego, La Jolla, CA, and approved February 16, 2018 (received for review December 15, 2017)

Disturbed RNA processing and subcellular transport contribute to the pathomechanisms of motoneuron diseases such as amyotrophic lateral sclerosis and spinal muscular atrophy. RNA-binding proteins are involved in these processes, but the mechanisms by which they regulate the subcellular diversity of transcriptomes, particularly in axons, are not understood. Heterogeneous nuclear ribonucleoprotein R (hnRNP R) interacts with several proteins involved in motoneuron diseases. It is located in axons of developing motoneurons, and its depletion causes defects in axon growth. Here, we used individual nucleotide-resolution cross-linking and immunoprecipitation (iCLIP) to determine the RNA interactome of hnRNP R in motoneurons. We identified ∼3,500 RNA targets, predominantly with functions in synaptic transmission and axon guidance. Among the RNA targets identified by iCLIP, the noncoding RNA 7SK was the top interactor of hnRNP R. We detected 7SK in the nucleus and also in the cytosol of motoneurons. In axons, 7SK localized in close proximity to hnRNP R, and depletion of hnRNP R reduced axonal 7SK. Furthermore, suppression of 7SK led to defective axon growth that was accompanied by axonal transcriptome alterations similar to those caused by hnRNP R depletion. Using a series of 7SK-deletion mutants, we show that the function of 7SK in axon elongation depends on its interaction with hnRNP R but not with the PTEF-B complex involved in transcriptional regulation. These results propose a role for 7SK as an essential interactor of hnRNP R to regulate its function in axon maintenance.

motoneuron | axon | iCLIP | 7SK | hnRNP R

Members of the heterogeneous nuclear ribonucleoprotein (hnRNP) family of RNA-binding proteins bind to nascent RNA and are implicated in all aspects of (pre)mRNA processing including transcription, splicing, stabilization, subcellular transport, translational control, and degradation (1). While hnRNPs have been investigated for their roles in splicing and gene expression, relatively little is known about their functions in regulating subcellular transcriptome diversity. This appears to be of particular importance for neurons whose axon extensions contain a complex repertoire of RNAs, which, via local translation, contribute to a number of neuronal responses such as axon guidance and maintenance. Thus, RNA-binding proteins might coordinate such processes through regulating the spatial availability of certain RNAs within axons (2).

The RNA-binding protein hnRNP R is located in the nucleus as well as in the cytosol of neurons. It is enriched in axons and axon terminals of motoneurons both in cell culture and in vivo (3, 4). Knockdown of hnRNP R in primary embryonic motoneurons reduces axon growth while dendrite length and survival of neurons remain unaffected (3). Similarly, in zebrafish embryos, morpholino-mediated knockdown of hnRNP R leads to reduced axon extension and massive alterations in axonal pathfinding, whereas neuronal survival is unimpaired. Even though these observations suggest that hnRNP R exerts specific roles in axon growth and integrity, the mechanism through which hnRNP R influences axon growth is still unclear. The RNA-binding activity of hnRNP R as well as its presence in axons points to the possibility that hnRNP R modulates the axonal abundance of distinct RNAs. In fact, *β-actin* mRNA has already been identified as an interactor of hnRNP R, and its transport into axons was found to depend on hnRNP R binding to its 3′ UTR (5). Importantly, hnRNP R interacts with a number of proteins linked to motoneuron diseases. Among these are Smn, a deficiency of which causes spinal muscular atrophy (SMA), and proteins associated with amyotrophic lateral sclerosis (ALS) such as TDP-43, FUS, MATR3, hnRNPA2B1, and hnRNPA1 (6–9).

Here we investigated the RNA interactome of hnRNP R by individual nucleotide-resolution cross-linking and immunoprecipitation (iCLIP) (10). Strikingly, we found the noncoding RNA 7SK as the main target of hnRNP R. 7SK is a 331-nt abundant nuclear RNA which regulates transcription. With the help of HEXIM1, 7SK sequesters the positive transcription elongation factor b (P-TEFb), a kinase complex composed of CDK9 and cyclin T1 (11, 12). P-TEFb stimulates transcription by phosphorylating the negative transcription elongation factors NELF and DSIF and by phosphorylating the C-terminal domain of paused polymerase II

Significance

Neurons are highly polarized cells. RNA-binding proteins contribute to this polarization by generating diverse subcellular transcriptomes. The RNA-binding protein hnRNP R is essential for axon growth in motoneurons. This study reports the RNA interactome for hnRNP R. The main interacting RNA of hnRNP R was the noncoding RNA 7SK. Depletion of 7SK from primary motoneurons disturbed axon growth. This effect was dependent on the interaction of 7SK with hnRNP R. Both hnRNP R and 7SK localize to axons. Loss of 7SK led to a similar depletion of axonal transcripts as loss of hnRNP R. Our data suggest that 7SK, in addition to its role in transcriptional regulation, acts in concert with hnRNP R to sort specific transcripts into axons.

Author contributions: M.B., L.S.-B., C.J., and M.S. designed research; M.B., L.S.-B., C.J., M.M., and H.G. performed research; M.U., S.A., and R.B. contributed new reagents/analytic tools; M.B., L.S.-B., C.J., M.M., H.G., M.U., S.A., and R.B. analyzed data; and M.B., L.S.-B., C.J., and M.S. wrote the paper.

The authors declare no conflict of interest.

This article is a PNAS Direct Submission.

Data deposition: The data discussed in this publication have been deposited in the National Center for Biotechnology Information Gene Expression Omnibus database (GEO Series accession no. GSE77101).

[1]M.B., L.S.-B., and C.J. contributed equally to this work.

[2]To whom correspondence should be addressed. Email: Sendtner_M@ukw.de.

This article contains supporting information online at www.pnas.org/lookup/suppl/doi:10.1073/pnas.1721670115/-/DCSupplemental.

Published online March 5, 2018.

(Pol II) (13). More recently, the hnRNPs A1, A2/B1, R, and Q have been shown to interact with the fraction of 7SK RNA not bound to P-TEFb, thereby forming distinct 7SK/hnRNP complexes (14–16). It has been suggested that the relative balance between 7SK/P-TEFb and 7SK/hnRNP complexes determines the amount of free P-TEFb, which, in turn, regulates the transcriptional output of a cell (17). Nevertheless, the function of individual 7SK/hnRNP complexes in general and in neuronal development in particular has remained unclear.

We show that 7SK localizes not only to the nucleus but also to the cytosol, including axons and growth cones of motoneurons, and that this localization is dependent on hnRNP R. Furthermore, we show that 7SK regulates axon growth in a manner dependent on hnRNP R binding. To elucidate the role of 7SK/hnRNP R complexes in axonal RNA transport, we analyzed the transcriptome of hnRNP R- and 7SK-knockdown motoneurons cultured in compartmentalized microfluidic chambers (18). As a result, we found a subset of transcripts that were up- or down-regulated similarly in axons of 7SK- and hnRNP R-knockdown motoneurons. Taken together, our results demonstrate that hnRNP R shapes the axonal transcriptome and suggest that its activity toward RNA localization is intricately linked to its main binding partner, 7SK.

Results

hnRNP R Binds to the 3′ UTR of mRNAs. To understand better the mechanisms by which hnRNP R modulates axon growth in motoneurons we used iCLIP (10) to identify RNAs interacting with hnRNP R on a genome-wide scale. We performed hnRNP R iCLIP on embryonic primary mouse motoneurons as well as on mouse NSC34 cells, which have been described previously as having motoneuron-like properties (19). For each cell type we prepared whole-cell lysates as well as one set of nuclear and cytosolic fractions (Fig. S1*A*). Through alternative splicing of exon 2, *hnRNP R* gives rise to two isoforms that differ at the N terminus. Therefore, for immunoprecipitation we applied an antibody specific for the C terminus of hnRNP R (hereafter referred to as "Ab1"), which identifies both the long and the short hnRNP R isoforms, as well as an antibody (hereafter referred to as "Ab2") specific for the N terminus of the longer isoform of hnRNP R. As negative control, we used rabbit IgG antibody for iCLIP from NSC34 cells. Compared with complete RNase digestion (++), partial RNase digestion (+) produced cross-linked protein–RNA complexes containing RNAs of variable size visible as a shift toward higher molecular weight (Fig. 1*A*). We isolated the RNA components from these complexes and processed the cross-linked RNAs for high-throughput sequencing (Table S1). A random barcode on each read was used to exclude effects from PCR amplification (10). Thus, for reads with identical barcodes mapping to the same genomic start location, only the separate barcodes are counted and quantified as cDNA counts. The nucleotide upstream of a read is defined as the cross-link site. We observed a high gene-by-gene correlation of cDNA counts between the experimental replicates for each cell type as well as between the two hnRNP R antibodies, demonstrating the reproducibility of hnRNP R iCLIP (Table S2).

After combining the datasets for each cell type (Fig. S1*A*), we performed sequence analysis of the hnRNP R cross-link sites. The occurrence of individual pentamers around cross-link sites was highly similar in NSC34 cells and motoneurons (Fig. 1*B*). The most highly enriched pentamer in both cell types was AAATT. This pentamer was also enriched when hnRNP R was immunoprecipitated with Ab2 (Fig. S1*B*) but not when IgG was used (Fig. S1*C*). Pentamer occurrence was highly correlated between individual replicates including enrichment of the AAATT pentamer, thus further demonstrating the reproducibility of hnRNP R iCLIP

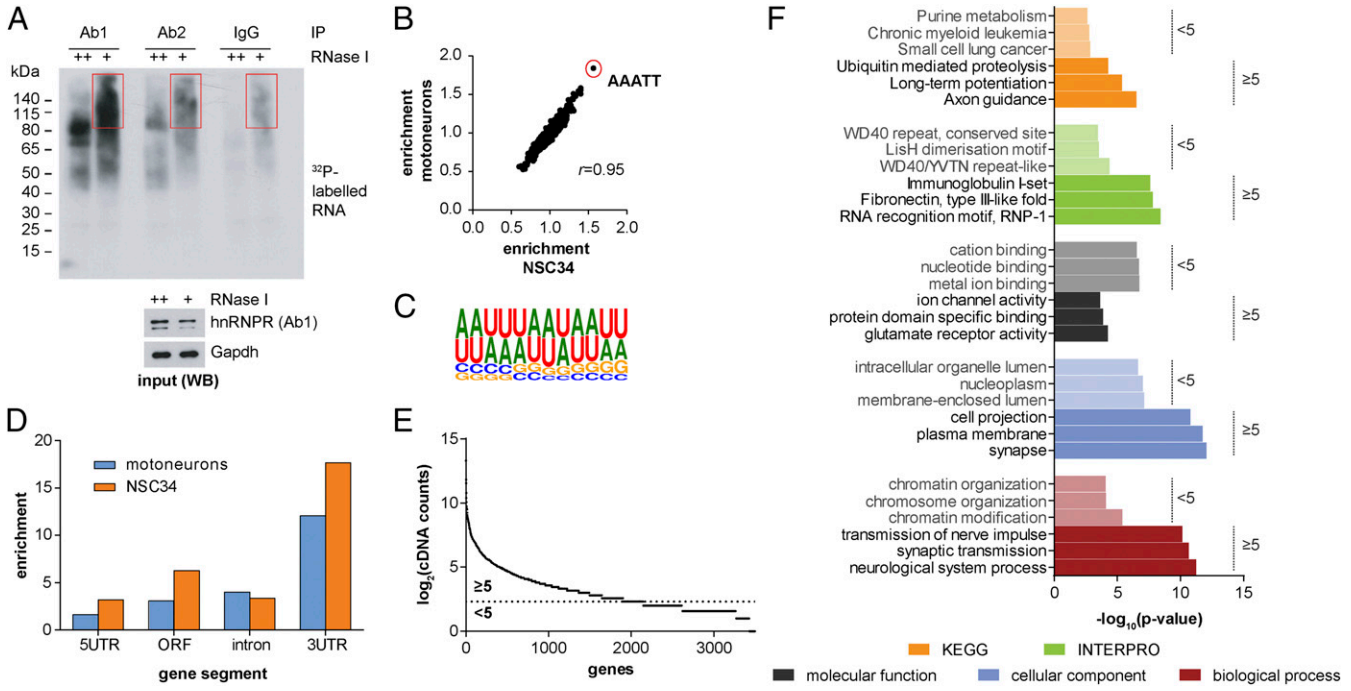

Fig. 1. Characterization of hnRNP R interactions with RNAs by iCLIP. (*A*, *Upper*) Autoradiogram of radiolabeled cross-linked hnRNP R–RNA complexes following immunoprecipitation from NSC34 cells with different hnRNP R antibodies. The red rectangles depict the area on the nitrocellulose from which protein–RNA complexes were purified for iCLIP cDNA amplification. Ab, antibody; IP, immunoprecipitation. (*Lower*) Western blot (WB) analysis of hnRNP R and Gapdh from the input lysates used for the immunoprecipitation. (*B*) Enrichment of pentamers around hnRNP R cross-link sites in motoneurons and NSC34 cells. The Pearson correlation coefficient (*r*) is shown. (*C*) GraphProt consensus motif at hnRNP R cross-link sites in motoneurons. (*D*) Enrichment of hnRNP R iCLIP cDNA counts in protein-coding transcripts. (*E*) Distribution of cDNA counts for the 3,493 hnRNP R iCLIP targets in motoneurons. (*F*) GO term, Kyoto Encyclopedia of Genes and Genomes (KEGG), and InterPro analysis of motoneuron transcripts containing greater than or equal to or fewer than five hnRNP R iCLIP cDNA counts in the combined dataset following cluster analysis.

(Fig. S1*D*). We also used an independent approach by learning binding models on the different datasets using GraphProt (20). The binding model for the hnRNP R iCLIP dataset similarly revealed an A/U-rich consensus motif (Fig. 1*C*) in contrast to the model learned from the IgG control iCLIP dataset (Fig. S1*E*).

Within genes, cross-links were enriched in annotated 3′ UTRs (Fig. 1*D*). As an example, hnRNP R cross-links were present in the 3′ UTR of *β-actin* at similar locations in motoneurons and NSC34 cells (Fig. S2*A*). The zipcode region, which is normally bound by Zbp1 (21), was devoid of cross-links (Fig. S2*B*). When we analyzed the distribution of hnRNP R cross-links separately for the individual experiments, we found that intronic iCLIP hits were mainly identified in the nuclear fractions, whereas interactions of hnRNP R with 3′ UTRs were enriched in the cytosolic fractions (Fig. S2*C*). This indicates that nuclear hnRNP R associates with nascent RNAs while cytoplasmic hnRNP R specifically targets the 3′ UTR of mRNAs, as previously observed for other members of the hnRNP family such as TDP-43 (22).

To obtain high-confidence RNA interactors, we filtered the transcripts cross-linked to hnRNP R in motoneurons and NSC34 cells using two stringent criteria. First, we used peak finding of the combined iCLIP data to detect significant clusters of hnRNP R-binding sites (23). Second, we considered only genes having iCLIP hits in all three replicates (combining the respective nuclear and cytosolic datasets as one replicate). As a result, we detected 3,493 transcripts in motoneurons (Dataset S1) and 2,932 transcripts in NSC34 cells (Dataset S2) as hnRNP R targets. To obtain functional information about these transcripts, we performed gene ontology (GO) term analysis separately on transcripts with five or more or fewer than five total clustered cDNA counts (Fig. 1*E*). This analysis revealed an enrichment of transcripts with functions in synaptic transmission and RNA binding among those transcripts more frequently bound by hnRNP R (Fig. 1*F*).

hnRNP R Modulates the Axonal Transcriptome. Given the important role of hnRNP R in axonal *β-actin* mRNA translocation (3), the location of hnRNP R cross-link sites in the 3′ UTR of mRNAs points toward a function of hnRNP R in regulating subcellular RNA levels. To study subcellular transcriptome alterations upon loss of hnRNP R, we virally transduced an shRNA to knock down hnRNP R in embryonic primary mouse motoneurons cultured in microfluidic chambers (18). After 7 d in vitro (DIV) RNA was extracted from the somatodendritic and axonal compartments of four independent control and three independent hnRNP R-knockdown motoneuron cultures. Under this condition hnRNP R transcripts were knocked down to <50% relative to controls as measured by qPCR (Fig. 2*A*). To investigate transcriptome alterations in each compartment, we applied a whole-transcriptome amplification strategy followed by high-throughput sequencing (24). The knockdown of hnRNP R transcripts measured by RNA sequencing (RNA-seq) was in concordance with the qPCR analysis (Fig. 2*A*). To detect transcripts altered upon hnRNP R knockdown in the somatodendritic and axonal compartments, we performed differential-expression analysis (Fig. 2*B*). We found 159 transcripts up-regulated (Dataset S3) and 181 transcripts significantly down-regulated ($P < 0.05$) (Dataset S4) in the somatodendritic compartment of motoneurons depleted for hnRNP R relative to controls. In the axonal compartment, the levels of 110 transcripts were increased

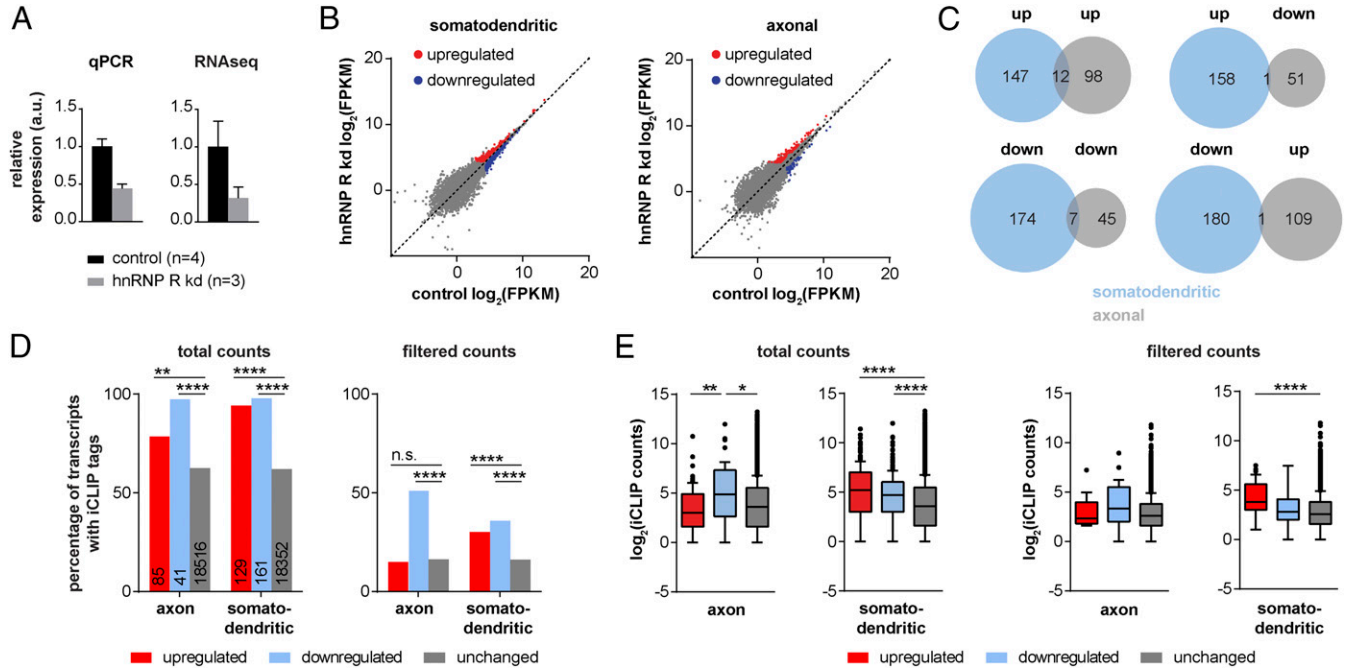

Fig. 2. hnRNP R depletion alters the somatodendritic and axonal transcriptome of motoneurons. (*A*) *hnRNP R* transcript levels on the somatodendritic side of compartmentalized hnRNP R-knockdown (kd) motoneurons relative to controls. Levels are shown as relative expression measured by qPCR or whole-transcriptome RNA-seq. Data represent mean ± SD. (*B*) Differential-expression analysis of compartmentalized hnRNP R-knockdown motoneurons. Scatter plots show logarithmized fragments per kilobase of transcript per million mapped reads (FPKM) values as reported by cuffdiff for whole-transcriptome RNA-seq of hnRNP R-knockdown motoneurons relative to controls. (*C*) Overlap of transcripts significantly ($P < 0.05$) deregulated in the somatodendritic and axonal compartments of hnRNP R-knockdown motoneurons. (*D*) hnRNP R binding to transcripts deregulated in hnRNP R-knockdown motoneurons. The bar graph shows the percentage of transcripts containing at least one iCLIP hit. For the analysis grouped hnRNP R iCLIP motoneuron data (total counts) or data from stringently filtered transcripts containing clusters of iCLIP hits as well as iCLIP hits in all three replicates (filtered counts) were used. Unchanged transcripts are defined as having a $P \geq 0.05$. Numbers on the bars represent the total number of transcripts considered. $^{**}P \leq 0.01$, $^{****}P \leq 0.0001$; n.s., not significant; χ^2 test with Yates' correction. (*E*) Tukey box plots showing the number of iCLIP hits per transcript. Only transcripts with at least one iCLIP hit were considered for the analysis. $^{*}P \leq 005$, $^{**}P \leq 0.01$, $^{****}P \leq 0.0001$; Kruskal–Wallis ANOVA with Dunn's multiple comparison test.

(Dataset S5), and 52 transcripts were reduced upon hnRNP R knockdown (Dataset S6). Among the deregulated transcripts, 12 were up-regulated in both compartments, and seven were reduced in both compartments after hnRNP R suppression (Fig. 2*C*). Thus, only a minority of transcripts are altered on both the somatodendritic and axonal sides upon hnRNP R loss, while most are unique to each compartment. Nevertheless, GO term analysis revealed that transcripts with functions in translation were enriched in either compartment among up-regulated RNAs (Fig. S3*A*). We validated a number of axonal transcript changes by qPCR (Fig. S3*B*). Despite variability, which is to be expected for low-input amounts of RNA, the direction of change was in agreement with the changes predicted from the differential-expression analysis. The candidates selected for validation included the most strongly reduced protein-coding transcripts *Sh2d3c* and *Ppfia3*, the transcript *Apoe*, which is up-regulated in ALS mice (25, 26), and the transcripts *Cald1*, *Nes*, and *Pls3* with functions in axon growth (27–29).

Next, we analyzed the occurrence of iCLIP hits in transcripts that were differentially expressed in hnRNP R-knockdown motoneurons. Among axonal transcripts, 98% of the transcripts down-regulated upon hnRNP R knockdown contained iCLIP hits, compared with 79% of the up-regulated and 62% of the unchanged transcripts (Fig. 2*D*, total counts). The enrichment of hnRNP R binding to down-regulated transcripts was also observed when we considered only the high-confidence RNA interactors of hnRNP R (see above). In this case 51% of down-regulated transcripts contained clustered iCLIP binding sites, compared with 15% of the up-regulated and 16% of the unchanged transcripts (Fig. 2*D*, filtered counts). For somatodendritic transcripts, 95% of the up-regulated and 98% of the down-regulated transcripts contained iCLIP hits compared with 62% of the unchanged ones. When we considered stringently filtered iCLIP hits, 30% of the up-regulated, 36% of the down-regulated, and 16% of the unchanged transcripts contained hnRNP R-binding clusters. Likewise, when we analyzed the total number of iCLIP hits per transcript, we found that axonal transcripts down-regulated upon hnRNP R knockdown contained significantly more iCLIP hits than up-regulated or unchanged ones (Fig. 2*E*). In the somatodendritic compartment up- as well as down-regulated transcripts contained significantly more iCLIP hits compared with unchanged ones. Thus, hnRNP R regulates the somatodendritic as well as axonal levels of a subset of its RNA targets.

7SK Is the Main Interacting RNA of hnRNP R. When the hnRNP R RNA targets in motoneurons were overlapped with those in NSC34 cells, 1,481 transcripts were common to both cell types (Fig. 3*A*). Strikingly, the small noncoding RNA 7SK was the highest-ranked binding partner for hnRNP R in both NSC34 cells and motoneurons (Fig. 3*B*). The pattern of iCLIP hits along 7SK RNA was highly similar in NSC34 cells and motoneurons, showing three distinct clusters (Fig. 3*C*). Their positions at nucleotide resolution were virtually identical for both cell types (Fig. S4*A*) and were located in stem loops (SL) 1 and 3 (Fig. S4*B*).

Since 7SK RNA is ubiquitously expressed and highly abundant, we investigated an iCLIP dataset for the unrelated RNA-binding protein Celf4 in mouse brain (30). The fraction of cDNA counts derived from Celf4 cross-links to 7SK (transcript ENSMUSG00000065037) is much smaller than the fraction of 7SK-derived cDNA counts in our hnRNP R iCLIP motoneuron datasets (7.5×10^{-5} for Celf4 iCLIP vs. 8.9×10^{-3} for hnRNP R iCLIP). In contrast, the fractions of cDNA counts for the abundant long noncoding RNAs *Malat1* and *Meg3* are similar in the Celf4 and hnRNP R datasets [7.9×10^{-3} (*Malat1*) and 3.1×10^{-3} (*Meg3*) for Celf4 iCLIP vs. 4.8×10^{-3} (*Malat1*) and 5.1×10^{-3} (*Meg3*) for hnRNP R iCLIP], indicating the specificity of hnRNP R binding to 7SK. Furthermore, in NSC34

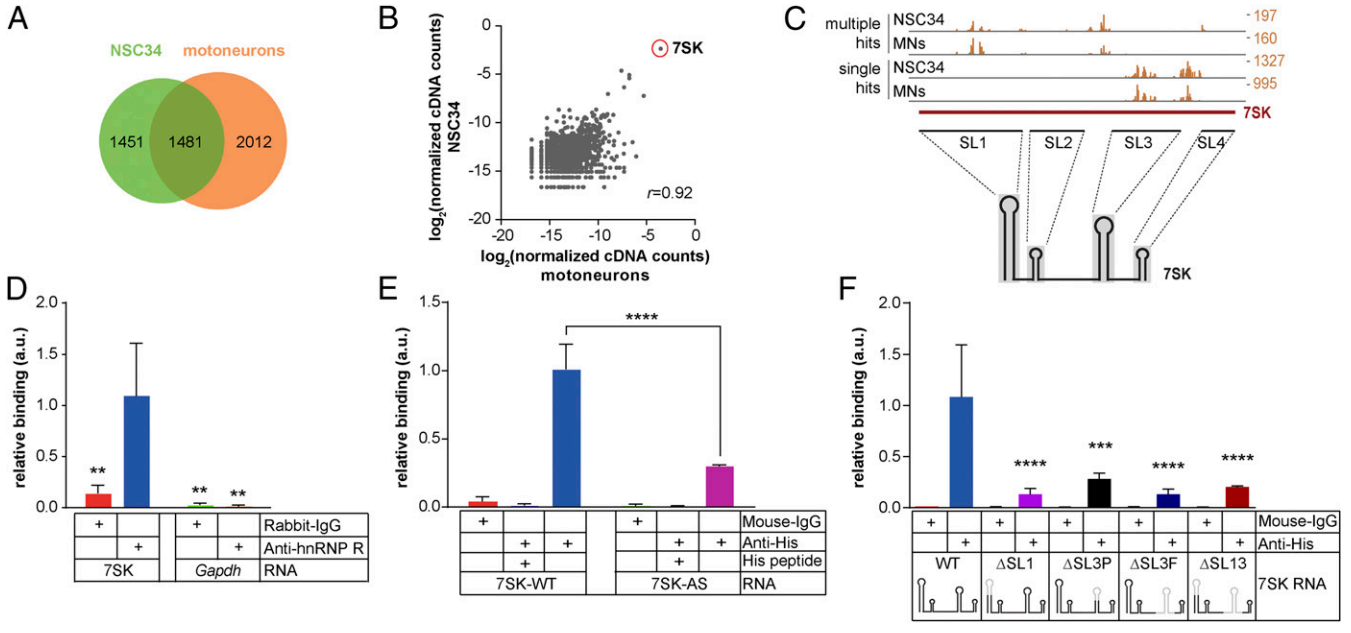

Fig. 3. 7SK RNA is the main interactor of hnRNP R. (*A*) Venn diagram of RNAs cross-linked to hnRNP R in NSC34 cells and motoneurons. (*B*) Scatter plot showing the normalized logarithmized hnRNP R iCLIP cDNA counts per transcript in both NSC34 cells and motoneurons. For normalization, cDNA counts within individual genes were normalized by the total number of cDNA counts. Pearson's *r* is shown. (*C*) Distribution of hnRNP R iCLIP cDNA counts along 7SK RNA (ENSMUSG00000065037). Due to 7SK being present as multiple copies in the genome, iCLIP reads mapping as single and multiple hits were considered. MNs, motoneurons. (*D*) RNA immunoprecipitation of hnRNP R from NSC34 cell lysate. As a negative control rabbit IgG antibody was used. 7SK RNA and *Gapdh* mRNA were detected by qPCR. (*E*) RNA immunoprecipitation of hnRNP R from in vitro binding reactions containing recombinant His-tagged hnRNP R and either 7SK RNA (7SK-WT) or its antisense version (7SK-AS) as negative control. To control for specificity of the immunoprecipitation, mouse IgG antibody was used or an excess of His peptide was included in the hnRNP R immunoprecipitation. (*F*) RNA immunoprecipitation of hnRNP R from in vitro binding reactions containing recombinant His-tagged hnRNP R and 7SK RNAs harboring the indicated mutations. A schematic representation of the 7SK RNAs is shown with deleted regions depicted in gray. Data in *D*–*F* are mean ± SD; $^{**}P \leq 0.01$, $^{***}P \leq 0.001$, $^{****}P \leq 0.0001$; two-way ANOVA with Tukey's multiple comparisons test.

cells the fraction of hnRNP R iCLIP cDNA counts in 7SK is 2.7×10^{-2} (*Malat1*: 1.7×10^{-3}) for Ab1 and 2.5×10^{-2} (*Malat1*: 2.0×10^{-3}) for Ab2, whereas the fraction of 7SK-derived cDNA counts in the IgG iCLIP control dataset from NSC34 cells is lower, at 1.0×10^{-3} (*Malat1*: 2.2×10^{-3}).

To validate that hnRNP R and 7SK interact in vivo, we immunoprecipitated hnRNP R from NSC34 cell lysate and investigated bound RNAs by qPCR. As a result, we detected 7SK, but not *Gapdh*, in the immunoprecipitate (Fig. 3*D*). Next, we sought to verify that hnRNP R and 7SK interact directly. For this purpose we set up in vitro binding reactions containing recombinant His-tagged hnRNP R and either 7SK or its antisense RNA. We immunoprecipitated hnRNP R from these binding reactions using an anti-His antibody and found that 7SK, but not its antisense RNA, coprecipitated with hnRNP R (Fig. 3*E*). Thus, hnRNP R directly interacts with 7SK. Since we detected most of the hnRNP R cross-links in SL1 and SL3, we generated 7SK RNAs with deletions in these regions and tested their ability to bind hnRNP R (Fig. 3*F*). All deletions, including either partial (ΔSL3P) or full (ΔSL3F) deletion of SL3, significantly reduced 7SK binding to hnRNP R. Taken together, these data confirm that hnRNP R binds to 7SK via interactions with SL1 and 3.

To investigate whether SL1 and 3 of 7SK also mediate binding to hnRNP R in vivo, we generated a series of knockdown constructs expressing an shRNA targeting 7SK and coexpressing the 7SK deletion mutants tested for in the in vitro binding to hnRNP R (Fig. 4*A*). Additionally, a construct was generated coexpressing a knockdown-resistant 7SK (7SK-MM3) with mismatches in the region targeted by the shRNA. We transfected NSC34 cells with these plasmids and used the cell lysates for RNA immunoprecipitation of hnRNP R. Since transfection of cells was only partial, the cell lysate contained endogenous 7SK from untransfected cells as well as 7SK mutant RNA from transfected cells in which endogenous 7SK was knocked down. Therefore, RNA immunoprecipitation of hnRNP R allowed assessment of the binding of each 7SK mutant to hnRNP R relative to the binding of endogenous 7SK. Using this assay, we found that 7SK-MM3 RNA was able to bind to hnRNP R in vivo (Fig. 4*B*). In agreement with our in vitro binding assay, we observed strongly reduced binding of hnRNP R to 7SK RNAs with deletion of SL1 (ΔSL1), full deletion of SL3 (ΔSL3F), or deletions of both SL1 and 3 (ΔSL13). However, 7SK RNA with partial deletion of SL3 (ΔSL3P) retained its ability to bind to hnRNP R under these conditions. Thus, the interaction of hnRNP R with 7SK in vivo also requires SL1 and SL3.

hnRNP R Regulates the Subcellular Localization of 7SK. Even though 7SK is an abundant nuclear RNA, we found cross-linked 7SK/hnRNP R complexes enriched in the cytosolic fractions of both motoneurons and NSC34 cells (Fig. 5*A*). These 7SK/hnRNP R complexes could be immunoprecipitated with both Ab1 and Ab2. In contrast, interactions with the abundant long noncoding RNAs *Malat1* and *Xist* were mainly observed in the nuclear fractions, corresponding to their known nuclear localization. This result suggests that 7SK/hnRNP R complexes translocate from the nucleus to the cytosol. In a previous study using compartmentalized motoneurons, we detected 7SK in axons of cultured motoneurons (24). Using in situ hybridization, we found that the cytosolic localization of 7SK extends not only into axons but even into the growth cones of motoneurons (Fig. 5*B*). In axons, we observed 7SK-positive punctae in close proximity to hnRNP R-labeled structures (Fig. 5 *C* and *D*). Thus, while being located mainly in the nucleus, both 7SK and hnRNP R localize to axons of developing motoneurons.

Since 7SK is the main RNA target for hnRNP R, we examined a putative role for hnRNP R in regulating the cytosolic localization of 7SK by using lentiviral knockdown of hnRNP R in motoneurons. After 5 DIV hnRNP R protein levels were reduced by ∼90% for the long isoform and ∼70% for the short isoform (Fig. 5*E*). hnRNP R RNA levels were similarly reduced, while total 7SK levels were

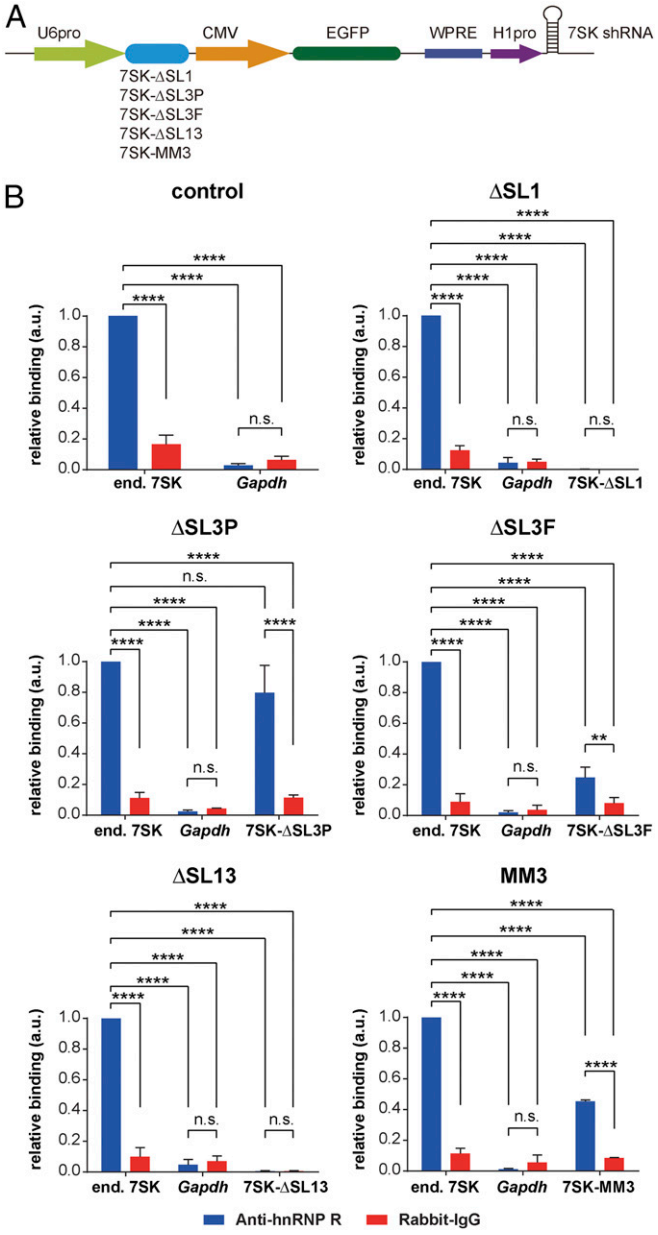

Fig. 4. Interaction of hnRNP R with 7SK in vivo. (*A*) Schematic representation of the constructs for expressing an shRNA from the H1 promoter (H1pro) targeting 7SK and coexpressing 7SK mutants harboring deletions (7SK-ΔSL1, ΔSL3P, ΔSL3F, and ΔSL13) or substitutions in the region targeted by the shRNA (7SK-MM3). The mutant 7SK RNAs are transcribed by the U6 promoter (U6pro). Expression of EGFP was used for assessing transfection efficiency. (*B*) RNA immunoprecipitations of hnRNP R from lysates of NSC34 cells transfected with the constructs shown in *A*. As control, empty plasmid was used. To control for specificity of the immunoprecipitations, rabbit IgG antibody was used, and precipitated RNA was tested for the presence of *Gapdh* by qPCR. Data are mean ± SD; $^{**}P \leq 0.01$, $^{****}P \leq 0.0001$; n.s., not significant; two-way ANOVA with Tukey's multiple-comparisons test. end., endogenous.

unaffected by hnRNP R knockdown (Fig. 5*F*). Quantification of 7SK levels in the nuclei of hnRNP R-knockdown motoneurons revealed no significant alterations (Fig. 5*G*), whereas 7SK-positive punctae almost completely disappeared from axons upon loss of hnRNP R (Fig. 5*H*). Thus, hnRNP R depletion does not alter nuclear 7SK levels but selectively reduces axonal levels of 7SK RNA in motoneurons.

7SK Regulates Axon Growth in an hnRNP R-Dependent Manner. hnRNP R has previously been implicated in axon growth and guidance (3).

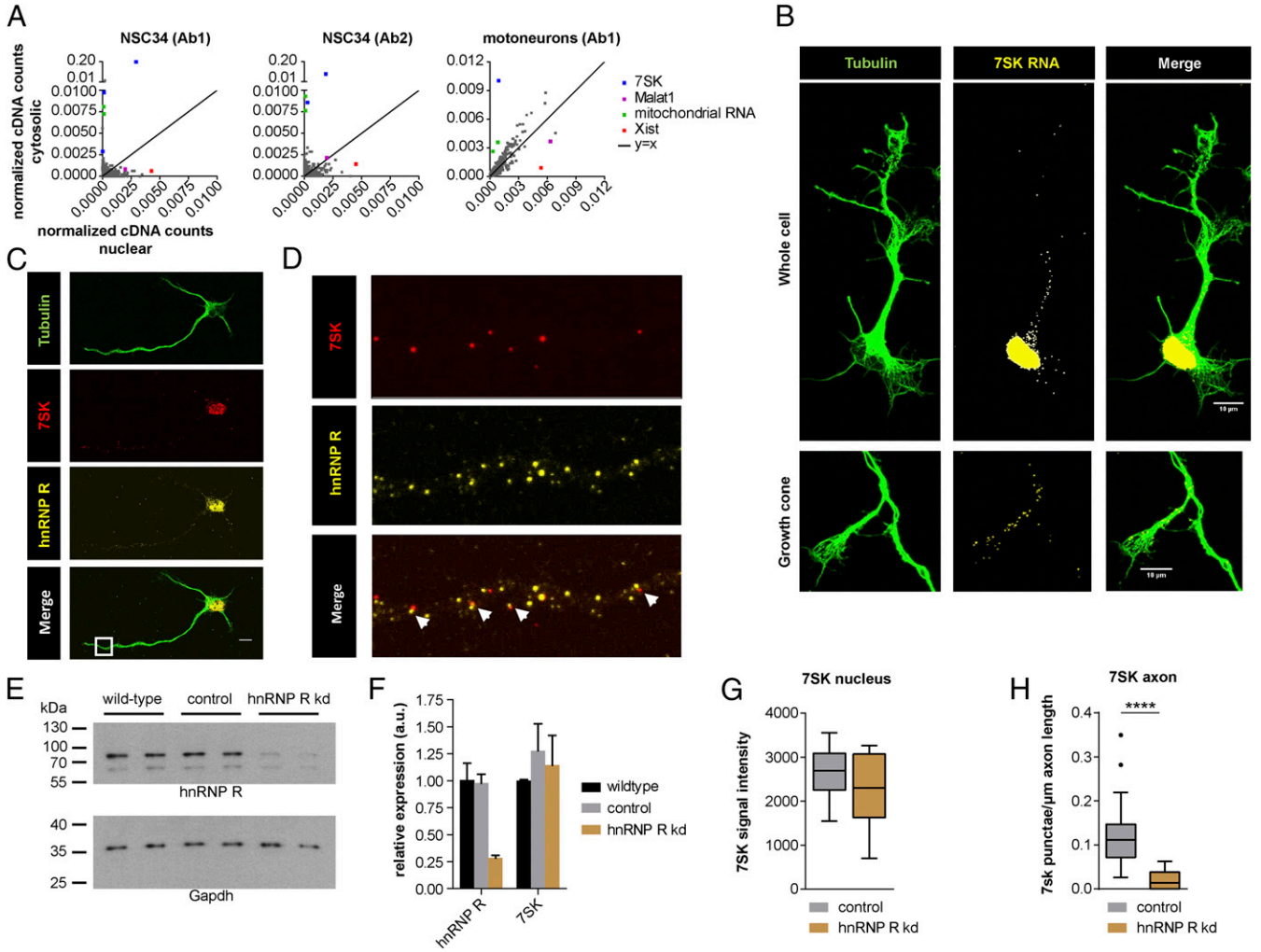

Fig. 5. hnRNP R regulates the subcellular distribution of 7SK in motoneurons. (*A*) Scatter plots depicting the fraction of hnRNP R iCLIP cDNA counts for individual genes within the nuclear and cytosolic fraction. Multiple dots for a highlighted RNA indicate different genes. (*B*) Subcellular localization of 7SK in motoneurons at 5 DIV detected by in situ hybridization. For visualization, cells were immunostained for tubulin. (Scale bars: 10 µm.) (*C*) 7SK labeling by in situ hybridization and immunostaining for hnRNP R in motoneurons. (Scale bar: 10 µm.) (*D*) Magnification of boxed area shown in *C*. Arrowheads show 7SK-positive punctae in close proximity to hnRNP R-positive structures. (*E*) Western blot detection of hnRNP R in wild-type, control, and hnRNP R-knockdown motoneurons cultured until 5 DIV. Gapdh was used as loading control. (*F*) qPCR of hnRNP R and 7SK from wild-type, control, and hnRNP R-knockdown motoneurons cultured for 5 DIV. Data are mean ± SD. (*G*) Tukey box plots of 7SK signal intensities in the nuclei of control and hnRNP R-knockdown motoneurons cultured for 5 DIV in two independent experiments. Median intensities are indicated by black horizontal lines. (*H*) Tukey box plots of the number of 7SK-positive punctae per µm axon in control and hnRNP R-knockdown motoneurons cultured for 5 DIV in two independent experiments. Median 7SK-positive punctae numbers are indicated by black horizontal lines. kd, knockdown. $n = 27$ for control and $n = 20$ for hnRNP R knockdown (*G* and *H*). $^{****}P \leq 0.0001$; Mann–Whitney test.

Since 7SK is the most prominent RNA target for hnRNP R, we investigated the effect of 7SK RNA depletion on axon growth. For this purpose we knocked down 7SK by lentiviral shRNA transduction and cultured the knockdown motoneurons until 7 DIV, a time point at which axons have reached a length often exceeding 500 µm. While 7SK RNA was substantially reduced in knockdown motoneurons (Fig. 6*A*), their survival was not affected (Fig. 6*B*). Compared with control axons reaching a median length of >400 µm after 7 DIV, 7SK knockdown motoneurons had shorter axons with a median length of ∼300 µm (Fig. 6 *C* and *D*). Thus, the observation that 7SK knockdown interferes with axon elongation but not with the survival of motoneurons in vitro is similar to the phenotype of hnRNP R depletion.

Next, we investigated whether the interaction between 7SK and hnRNP R is necessary for the role of 7SK in axon elongation. For this purpose we assessed the ability of the different 7SK mutant RNAs (Fig. 3*F*) to rescue axon growth after depletion of endogenous 7SK. We generated lentiviruses from the constructs expressing an shRNA against 7SK and coexpressing mutant 7SK (Fig. 4*A*) and transduced primary motoneurons to measure their axon lengths after 7 DIV. We found that wild-type 7SK, 7SK-MM3, and 7SK-ΔSL3P were able to restore axon extension in 7SK-knockdown motoneurons, while 7SK-ΔSL3F and 7SK-ΔSL1 failed to rescue this effect (Fig. 6*E*). Since 7SK-ΔSL3P but neither 7SK-ΔSL3F nor 7SK-ΔSL1 can bind to hnRNP R in vivo, this result suggests that 7SK regulates axon growth through hnRNP R binding.

An important function of 7SK is to regulate transcription by binding to the P-TEFb complex composed of CDK9 and cyclin T1. We used an RNA pulldown assay to test our 7SK mutant RNAs for their ability to bind to P-TEFb (Fig. 7*A*). We hybridized a biotinylated antisense oligonucleotide to 7SK wild-type or mutant RNAs and incubated this duplex with NSC34 lysate. Following immobilization to streptavidin beads, we investigated bound P-TEFb components by immunoblotting. The antisense oligonucleotide was able to bind to and pull down all 7SK mutants (Fig. 7*B*). Following incubation with cell lysate, wild-type 7SK was bound to Cdk9 and cyclin T1 as well as to Larp7, which is essential for 7SK stability (Fig.

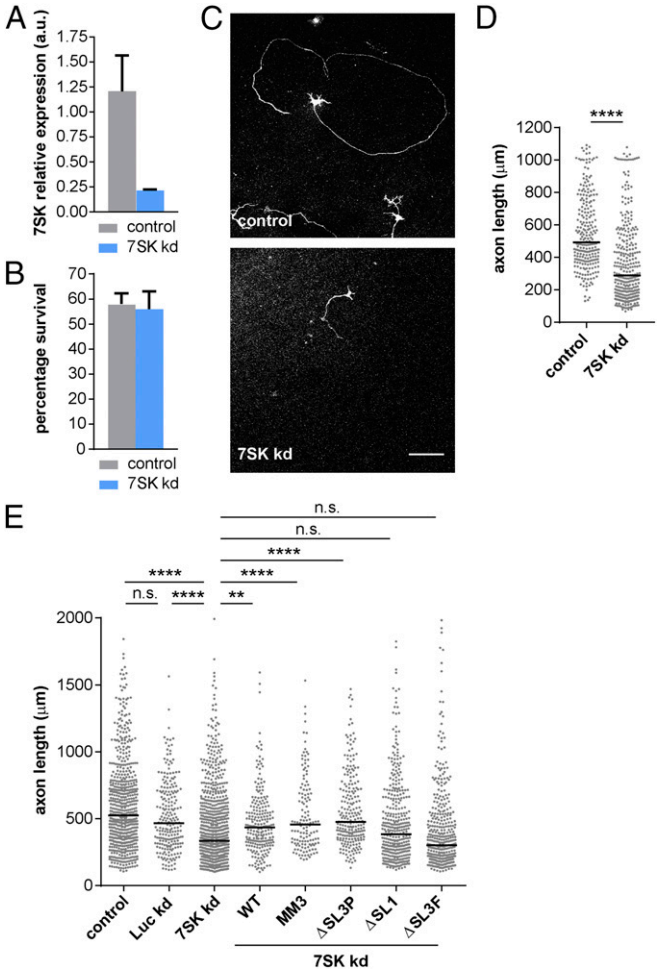

Fig. 6. 7SK lentiviral knockdown reduces axon length in cultured motoneurons. (*A*) qPCR of 7SK from control and 7SK-knockdown motoneurons cultured for 7 DIV. Data represent mean ± SD from two independent experiments. (*B*) Survival of control and 7SK-knockdown motoneurons after 7 DIV as percentage of the number of motoneurons at 1 DIV. Data represent mean ± SD from two independent experiments. (*C*) Examples of control and 7SK-knockdown motoneurons after 7 DIV. (Scale bar: 100 μm.) (*D*) Scatter plots showing the length of axons of control and 7SK-knockdown motoneurons cultured for 7 DIV. The median is indicated by a horizontal black line. $^{****}P \leq 0.0001$; Mann–Whitney test. (*E*) Scatter plots indicating the axon lengths of 7SK-knockdown motoneurons coexpressing different 7SK-mutant RNAs. As further control, an shRNA against luciferase (Luc kd) was expressed. $^{**}P \leq 0.01$, $^{****}P \leq 0.0001$; n.s., not significant; Kruskal–Wallis ANOVA with Dunn's multiple comparisons test.

7*C*) (31). As a negative control, 7SK antisense RNA purified with a biotinylated sense oligonucleotide did not copurify any of these components. Among the mutant 7SK RNAs, those mutants with deletion of SL1 (ΔSL1 and ΔSL13) failed to pull down Cdk9 or cyclin T1 (Fig. 7*C*). In contrast, mutants with deletions in SL3 (ΔSL3P and ΔSL3F) were able to bind to the P-TEFb components. This is in agreement with a previous report showing that P-TEFb is recruited to 7SK through SL1 and SL4 (32). Importantly, all mutants bound Larp7, indicating that they are otherwise stable. Taken together, our results suggest that the interaction of 7SK with hnRNP R is necessary for axon growth, since the 7SK mutant ΔSL3F is unable to rescue the axonal defect of 7SK-deficient motoneurons even though it is capable of binding to P-TEFb.

A Subset of Axonal Transcripts Is Similarly Altered After Knockdown of 7SK or hnRNP R. Our data point toward the possibility that hnRNP R and 7SK act in concert to regulate the subcellular transcriptome of motoneurons. Thus, we investigated subcellular transcriptome alterations in compartmentalized 7SK-knockdown motoneurons. For this purpose we extracted somatodendritic and axonal RNA from four independent 7SK-knockdown motoneuron cultures and performed whole-transcriptome profiling as before. 7SK levels were suppressed by ∼50% as measured by qPCR (Fig. 8*A*). Since our whole-transcriptome amplification method also captures nonpolyadenylated transcripts, including 7SK, we were able to detect its depletion by ∼50% in the RNA-seq data as well (Fig. 8*A*). Transcripts altered upon 7SK knockdown relative to controls were detected in the somatodendritic and axonal compartments by differential-expression analysis (Fig. 8*B*). In the somatodendritic compartment 162 transcripts were up-regulated (Dataset S7) compared with 137 transcripts that were down-regulated significantly ($P < 0.05$) (Dataset S8). In the axonal compartment 137 transcripts were up-regulated (Dataset S9), and 46 transcripts were down-regulated (Dataset S10).

Since 7SK has a function in transcriptional regulation by inactivating P-TEFb, we investigated the binding of NELF, DSIF, and Pol II to the promoter regions of the genes that were deregulated in the somatodendritic compartment of 7SK-knockdown motoneurons. For this purpose we analyzed ChIP-seq data for NELF, DSIF, and Pol II to quantify their interaction with the promoter regions of

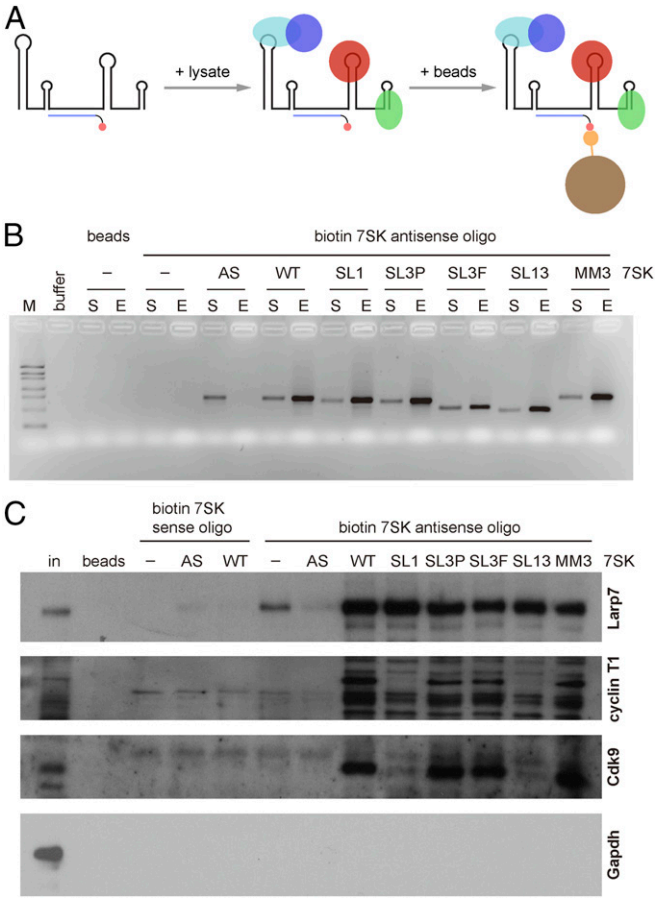

Fig. 7. Interaction of 7SK RNA-deletion mutants with P-TEFb. (*A*) Schematic representation of the RNA pulldown procedure. (*B*) Immobilization of in vitro-transcribed 7SK RNAs on streptavidin beads using a biotinylated antisense oligonucleotide. Agarose gel electrophoresis of the eluted RNA (E, 100% loading) and the RNA remaining in the supernatant (S, 10% loading). M, marker. (*C*) Western blot analysis of proteins bound to 7SK RNAs. As control, 7SK wild type (WT) and antisense (AS) were purified using either an antisense oligonucleotide that binds to wild type or a sense oligonucleotide that binds to antisense. in, input.

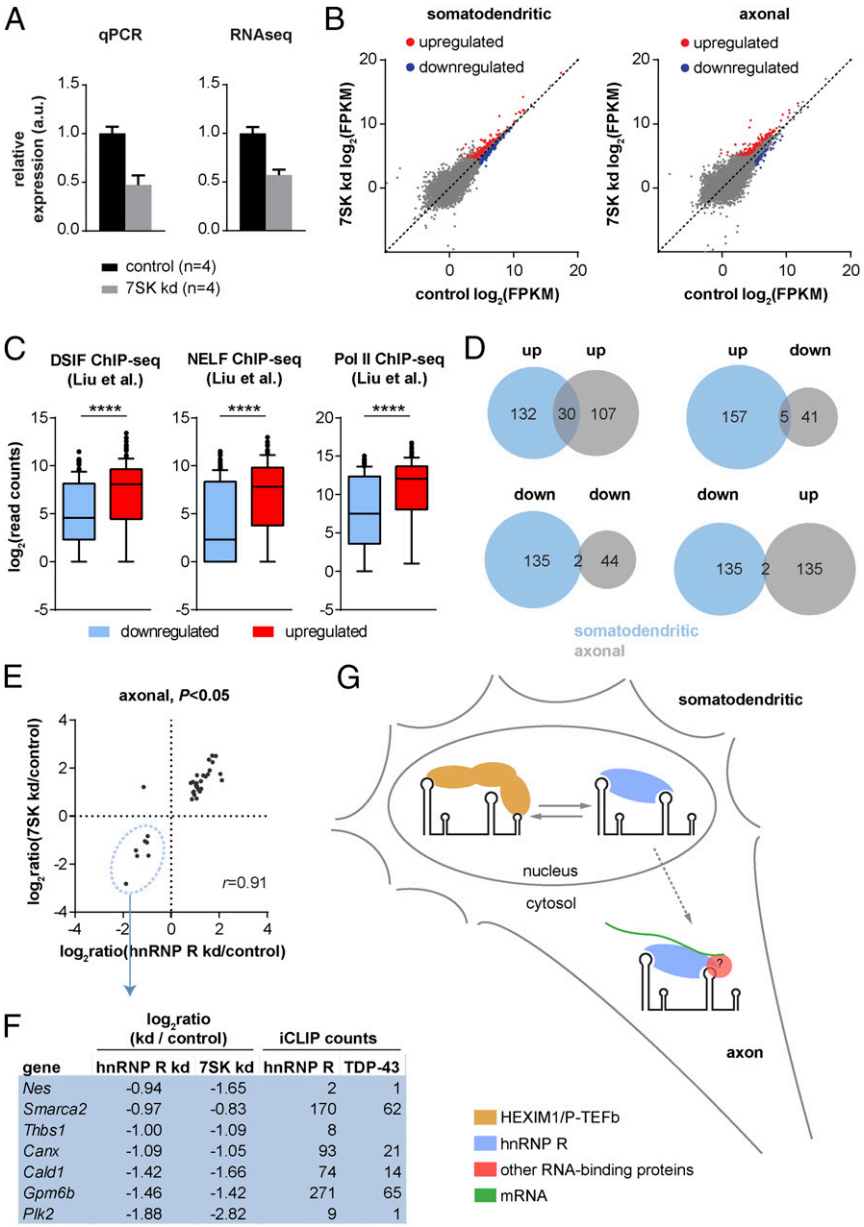

Fig. 8. Subcellular transcriptome alterations in 7SK-knockdown motoneurons. (*A*) 7SK levels measured by qPCR and whole-transcriptome RNA-seq in the somatodendritic compartment of 7SK-knockdown motoneurons. Data represent mean ± SD. (*B*) Differential expression analysis of 7SK-knockdown motoneuron compartments. (*C*) Tukey box plots showing the binding of DSIF, NELF, and Pol II from ChIP-seq data around the transcription start site (TSS) of transcripts significantly deregulated in the somatodendritic compartment of 7SK-knockdown motoneurons relative to controls. The ChIP-seq data were derived from Liu et al. (33). ****$P \leq 0.0001$; Mann–Whitney test. (*D*) Overlap of transcripts significantly ($P < 0.05$) deregulated in the somatodendritic and axonal compartments of 7SK-knockdown motoneurons. (*E*) Scatter plot showing logarithmized transcript fold change of axonal transcripts significantly ($P < 0.05$) deregulated in 7SK and hnRNP R-knockdown motoneurons. Pearson's *r* is shown. (*F*) List of transcripts significantly down-regulated in axons of hnRNP R-knockdown and 7SK-knockdown motoneurons. Included are the number of cDNA counts from the grouped motoneuron hnRNP R iCLIP dataset and the cDNA counts of TDP-43 iCLIP from human brain samples. kd, knockdown. (*G*) Model of 7SK/hnRNP R complex functions in motoneurons.

these genes (33). We found that transcripts up-regulated upon 7SK knockdown contain significantly more ChIP-seq reads for NELF, DSIF, and Pol II in their promoter region than down-regulated transcripts (Fig. 8*C*). Thus, in line with the function of 7SK in regulating P-TEFb activity, transcriptional up-regulation upon 7SK loss in motoneurons occurs for genes at which Pol II is stalled at promoters through NELF and DSIF binding.

Similar to hnRNP R knockdown in motoneurons, depletion of 7SK led to the deregulation of distinct subsets of transcripts in each compartment (Fig. 8*D*). Among RNAs up-regulated in axons of 7SK-depleted motoneurons, transcripts with functions in translation were enriched (Fig. S5*A*). Moreover, among transcripts down-regulated in axons of 7SK knockdown motoneurons, RNAs encoding proteins with cytoskeletal functions such as *Cald1*, *Nes*, *Csrp1*, and *Tpm1* were identified (Fig. S5 *A* and *B*). Thus, the observed axonal transcriptome alterations following 7SK knockdown resemble those occurring in axons of hnRNP R-knockdown motoneurons. Therefore, we investigated how the somatodendritic and axonal RNA-seq datasets for both knockdown conditions were related to each other. As a result, we found that the changes in levels of transcripts that were altered significantly under both knockdown conditions were strongly correlated (Fig. 8*E*

and Fig. S5*C*). This effect was particularly noticeable in the axonal compartment, where 37 transcripts were changed significantly upon either hnRNP R or 7SK knockdown. Of these, 29 transcripts were up-regulated and seven were down-regulated under both conditions (Fig. 8*E* and Table S3). Notably, among the transcripts up-regulated in axons after hnRNP R and after 7SK knockdown were several genes encoding ribosomal proteins as well as transcripts found to be up-regulated in spinal cord of patients with ALS, such as *Apoe*, *Fth1*, and *Ftl1* (25). In contrast, among the down-regulated RNAs were transcripts encoding proteins with functions in neurite growth such as *Cald1*, *Gpm6b*, and *Nes* (Table S3). The down-regulated transcripts were also found in the group of transcripts that were cross-linked to hnRNP R in motoneurons (Fig. 8*F*). As an example, hnRNP R cross-links were enriched in the 3′ UTR of *Gpm6b* (Fig. S5*D*) encoding a proteolipid protein involved in axon growth (34). Additionally, we examined a previously published iCLIP dataset for TDP-43, an hnRNP R interactor, in human control brains (22), and found that the down-regulated transcripts except *Thbs1* also contained cross-links to TDP-43 (Fig. 8*F*).

Discussion

Mechanisms for regulating subcellular RNA levels are involved in controlling the shape and function of the axonal compartment of neurons. Here we report that hnRNP R and its main interacting RNA, 7SK, regulate the RNA content of the somatodendritic and axonal compartment of motoneurons. Thus, our results provide evidence that RNA-binding proteins can act together with noncoding RNAs to regulate the subcellular abundance of transcripts underlying important cellular processes such as the differentiation and growth of axons.

The interactions identified by iCLIP suggest that hnRNP R binds to a large number of transcripts in motoneurons, many of which are associated with axon guidance and synapse functions. The binding sites of hnRNP R were enriched in the 3′ UTR, which points toward a role for hnRNP R in transcript subcellular transport and/or stability. Using compartmentalized motoneuron cultures combined with whole-transcriptome profiling, we found that loss of hnRNP R led to distinct transcriptome alterations in axons, including down-regulation of transcripts encoding proteins with cytoskeletal functions such as *Cald1*, *Nes*, and *Pls3*. Interestingly, PLS3 (plastin 3), an actin-bundling protein, has previously been identified as a modifier in SMA (29). Among up-regulated transcripts was *Apoe*, which is increased in the spinal cords of patients with ALS (25). Apoe overexpression causes cytoskeletal instability and disrupts axonal transport (35, 36). Based on these findings, future experiments must show whether the cytoskeletal integrity is disrupted in axons of hnRNP R-deficient motoneurons. Importantly, down-regulated but not up-regulated axonal transcripts were associated with significantly more hnRNP R iCLIP hits compared with unregulated transcripts. This suggests that the axonal transcripts down-regulated upon hnRNP R knockdown are those actively transported by hnRNP R, whereas those up-regulated, including many components of the translational machinery, might represent compensatory mechanisms. Additionally, the set of transcripts deregulated in the axonal compartment of hnRNP R-knockdown motoneurons was largely distinct from the transcript changes in the somatodendritic compartment. Thus, transcript alterations in the axons of knockdown motoneurons are not simply due to alterations in their abundance in the cell body but might rather reflect an active mechanism toward their transport or stability in axons.

When we evaluated the transcripts bound by hnRNP R in both NSC34 cells and motoneurons, the short noncoding RNA 7SK was the most highly enriched target. This is in agreement with previous reports identifying hnRNP R as a component of 7SK particles (14–16). Our iCLIP data add to this knowledge by showing that hnRNP R directly interacts with 7SK in vivo and that this interaction occurs within SL1 and SL3 of 7SK. We confirmed this interaction using an in vitro assay containing purified hnRNP R and different 7SK mutant RNAs. Additionally, we investigated hnRNP R binding to 7SK in vivo by RNA immunoprecipitation. Interestingly, while partial deletion of SL3 (ΔSL3P) abolished 7SK binding to hnRNP R in vitro, binding to hnRNP R in a cellular context was largely unaffected by this deletion. This suggests that hnRNP R recruitment to 7SK in cells might be supported by additional 7SK-interacting proteins. Nevertheless, complete removal of SL1 or SL3 abolished binding of hnRNP R both in vitro and in vivo, thereby confirming the functional relevance of the hnRNP R cross-linking sites in these regions.

Given that 7SK is the main interactor of hnRNP R, an important question is whether loss of 7SK similarly leads to reduced axon growth and whether such a defect depends on its interaction with hnRNP R. Indeed, we found that knockdown of 7SK in motoneurons led to reduced axon growth which resembles the axon growth defect following hnRNP R depletion. Furthermore, we were able to rescue this defect by coexpressing knockdown-resistant 7SK, which confirms the specificity of this phenotype. Importantly, a rescue effect was also observed by coexpression of the 7SK ΔSL3P but not of the ΔSL3F deletion mutant. Since ΔSL3P but not ΔSL3F can bind hnRNP R in vivo, this further indicates that the role of 7SK in axon elongation is mediated through 7SK/hnRNP R complexes. However, we cannot rule out the possibility that additional RNA-binding proteins interact with SL1 and/or SL3 and thereby regulate the functional role of 7SK in axon growth. Future experiments investigating the protein interactome of 7SK/hnRNP complexes in motoneurons will help resolve this question. Furthermore, while the 7SK mutant ΔSL3F did not bind hnRNP R, it was still able to recruit the P-TEFb complex. Given that 7SK ΔSL3F was unable to rescue the axonal defect of 7SK-knockdown motoneurons, this result points toward the possibility that a transcription-independent function of 7SK/hnRNP R complexes mediates this effect.

To further test the hypothesis that 7SK serves additional functions beyond modulating transcription (such as in regulating translocation of specific transcripts into the axon of motoneurons), we investigated transcriptome changes in compartmentalized 7SK-knockdown motoneuron cultures and compared them with those obtained after hnRNP R knockdown. This showed that a subset of axonal transcripts is regulated in a similar manner by hnRNP R and 7SK. Importantly, these transcripts also harbor hnRNP R cross-linking sites, which indicates that their axonal reduction in hnRNP R-knockdown motoneurons might be a direct consequence of hnRNP R deficiency and disassembly of 7SK/hnRNP R complexes. The down-regulated transcripts encode proteins known to play a role in axon growth and cytoskeleton assembly, suggesting a reason for the disturbed axon-elongation phenotype of motoneurons depleted of hnRNP R. One of these candidates, *Gpm6b*, has recently been implicated in axon growth and guidance. Gpm6b is a glycoprotein located in neurites, and Gpm6b-deficient neurons exhibit shorter axons in vitro and defective axon guidance in vivo (34, 37). Thus, the combined loss of *Gpm6b* and other transcripts encoding proteins with cytoskeletal functions, such as *Cald1*, might negatively affect axon growth. In contrast, several up-regulated transcripts encode ribosomal proteins. This finding is of interest, considering that an increased number of axonal ribosomes has been detected in a mouse model of ALS (38). Increased numbers of ribosomes might reflect a mechanism whereby an enhanced capacity for protein synthesis compensates for the reduced availability of functionally relevant transcripts. At the same time, up-regulation of specific ribosomal proteins might also have the opposite effect and disrupt ribosomes due to alterations of their stoichiometry (39). Future experiments directed toward measuring the rate of protein synthesis in hnRNP R- and 7SK-deficient motoneurons could help further clarify this point.

Interestingly, we also detected cross-linked 7SK/hnRNP R complexes in the cytosolic fractions of motoneurons, which indicates either that this complex that has originally been identified in the nucleus translocates to the cytosol or that 7SK and hnRNP R are

assembled into messenger ribonucleoprotein (mRNP) complexes once they have been transported independently to the cytosol. Since hnRNP R has been found to interact with a number of proteins linked to ALS, including TDP-43, it is tempting to speculate that transport mRNPs composed of 7SK/hnRNP R and other hnRNPs act in a cooperative manner to transport RNAs into axons or regulate their subcellular stability in axons (Fig. 8*G*). In agreement, we detected TDP-43 cross-links on those RNAs down-regulated in axons of hnRNP R- and 7SK-deficient motoneurons. Future studies directed toward identifying the RNA and protein composition of these particles will help unravel the mode of action of hnRNP R toward subcellular RNA localization.

Taken together, the close interaction of hnRNP R with 7SK and the similar repertoire of transcripts that are deregulated in axons of knockdown motoneurons indicate that 7SK and hnRNP R act together in the assembly and sorting of mRNP complexes for transcripts that are locally translated in axons to serve an essential role in axon growth.

Materials and Methods

Animals. CD-1 mice were housed in the animal facilities of the Institute of Clinical Neurobiology at the University Hospital of Wuerzburg. Mice were maintained in a 12-h/12-h day/night cycle under controlled conditions at 20–22 °C and 55–65% humidity with food and water in abundant supply. Experiments were performed strictly following the regulations on animal protection of the German federal law and of the Association for Assessment and Accreditation of Laboratory Animal Care, in agreement with and under control of the local veterinary authority and Committee on the Ethics of Animal Experiments (Regierung von Unterfranken).

Primary Mouse Motoneuron Culture. Motoneurons were prepared from E12.5 CD-1 mouse embryos as previously described (40). They were then cultured in microfluidic chambers using a BDNF gradient according to a published protocol (18).

iCLIP. iCLIP was performed as described previously (10). For subcellular fractionation, cells were lysed in fractionation buffer [50 mM Tris·HCl (pH 7.4), 100 mM NaCl, 0.1% Nonidet P-40].

RNA-Seq. For RNA-seq of compartmentalized motoneurons, we used a whole-transcriptome profiling method described previously (24).

RNA Immunoprecipitation. NSC34 cells were lysed [20 mM Tris·HCl (pH 7.5), 150 mM NaCl, 1.5 mM MgCl2, 2 mM DTT, 1% Nonidet P-40 buffer] followed by immunoprecipitation with anti-hnRNP R antibody (Abcam) or control rabbit IgG (Santa Cruz Biotechnology). Bound RNAs were extracted with TRIzol (Thermo Fisher), reverse-transcribed, and quantified by qPCR.

In Vitro Binding Assay. Protein G (Thermo Fisher) beads bound to anti-His antibody (Abgent) or control mouse IgG (Santa Cruz Biotechnology) were incubated with recombinant His-hnRNP R and 7SK RNAs generated by in vitro transcription in lysis buffer. Captured RNA was purified by proteinase K digestion and phenol-chloroform extraction, reverse-transcribed, and analyzed by qPCR.

RNA Pulldown Assay. 7SK RNAs generated by in vitro transcription were captured on Pierce streptavidin beads (Thermo Fisher) with a biotinylated antisense oligonucleotide and incubated with NSC34 cell lysate. Bound proteins were analyzed by SDS/PAGE and Western blotting.

A detailed description of the experimental and data analysis procedures can be found in *SI Materials and Methods*.

ACKNOWLEDGMENTS. We thank Črt Gorup and Tomaž Curk for bioinformatics support and Carsten Ade, Wolfgang Hädelt, and Victoria McParland for high-throughput sequencing. This work was supported by Deutsche Forschungsgemeinschaft program SPP1738 [Grants BR4910/1-1 (to M.B.), SE697/4-1 (to M.S.), and BA2168/11-1 (to R.B. and M.U.)] and program SPP1935 [Grants BR4910/2-1 (to M.B.) and SE697/5-1 (to M.S.)].

1. Dreyfuss G, Kim VN, Kataoka N (2002) Messenger-RNA-binding proteins and the messages they carry. *Nat Rev Mol Cell Biol* 3:195–205.
2. Buxbaum AR, Haimovich G, Singer RH (2015) In the right place at the right time: visualizing and understanding mRNA localization. *Nat Rev Mol Cell Biol* 16:95–109.
3. Glinka M, et al. (2010) The heterogeneous nuclear ribonucleoprotein-R is necessary for axonal beta-actin mRNA translocation in spinal motor neurons. *Hum Mol Genet* 19:1951–1966.
4. Dombert B, Sivadasan R, Simon CM, Jablonka S, Sendtner M (2014) Presynaptic localization of Smn and hnRNP R in axon terminals of embryonic and postnatal mouse motoneurons. *PLoS One* 9:e110846.
5. Rossoll W, et al. (2003) Smn, the spinal muscular atrophy-determining gene product, modulates axon growth and localization of beta-actin mRNA in growth cones of motoneurons. *J Cell Biol* 163:801–812.
6. Rossoll W, et al. (2002) Specific interaction of Smn, the spinal muscular atrophy determining gene product, with hnRNP-R and gry-rbp/hnRNP-Q: a role for Smn in RNA processing in motor axons? *Hum Mol Genet* 11:93–105.
7. Ling SC, et al. (2010) ALS-associated mutations in TDP-43 increase its stability and promote TDP-43 complexes with FUS/TLS. *Proc Natl Acad Sci USA* 107:13318–13323.
8. Hein MY, et al. (2015) A human interactome in three quantitative dimensions organized by stoichiometries and abundances. *Cell* 163:712–723.
9. Kamelgarn M, et al. (2016) Proteomic analysis of FUS interacting proteins provides insights into FUS function and its role in ALS. *Biochim Biophys Acta* 1862:2004–2014.
10. König J, et al. (2010) iCLIP reveals the function of hnRNP particles in splicing at individual nucleotide resolution. *Nat Struct Mol Biol* 17:909–915.
11. Yang Z, Zhu Q, Luo K, Zhou Q (2001) The 7SK small nuclear RNA inhibits the CDK9/cyclin T1 kinase to control transcription. *Nature* 414:317–322.
12. Nguyen VT, Kiss T, Michels AA, Bensaude O (2001) 7SK small nuclear RNA binds to and inhibits the activity of CDK9/cyclin T complexes. *Nature* 414:322–325.
13. Zhou Q, Li T, Price DH (2012) RNA polymerase II elongation control. *Annu Rev Biochem* 81:119–143.
14. Barrandon C, Bonnet F, Nguyen VT, Labas V, Bensaude O (2007) The transcription-dependent dissociation of P-TEFb-HEXIM1-7SK RNA relies upon formation of hnRNP-7SK RNA complexes. *Mol Cell Biol* 27:6996–7006.
15. Van Herreweghe E, et al. (2007) Dynamic remodelling of human 7SK snRNP controls the nuclear level of active P-TEFb. *EMBO J* 26:3570–3580.
16. Hogg JR, Collins K (2007) RNA-based affinity purification reveals 7SK RNPs with distinct composition and regulation. *RNA* 13:868–880.
17. C Quaresma AJ, Bugai A, Barboric M (2016) Cracking the control of RNA polymerase II elongation by 7SK snRNP and P-TEFb. *Nucleic Acids Res* 44:7527–7539.
18. Saal L, Briese M, Kneitz S, Glinka M, Sendtner M (2014) Subcellular transcriptome alterations in a cell culture model of spinal muscular atrophy point to widespread defects in axonal growth and presynaptic differentiation. *RNA* 20:1789–1802.
19. Cashman NR, et al. (1992) Neuroblastoma x spinal cord (NSC) hybrid cell lines resemble developing motor neurons. *Dev Dyn* 194:209–221.
20. Maticzka D, Lange SJ, Costa F, Backofen R (2014) GraphProt: modeling binding preferences of RNA-binding proteins. *Genome Biol* 15:R17.
21. Ross AF, Oleynikov Y, Kislauskis EH, Taneja KL, Singer RH (1997) Characterization of a beta-actin mRNA zipcode-binding protein. *Mol Cell Biol* 17:2158–2165.
22. Tollervey JR, et al. (2011) Characterizing the RNA targets and position-dependent splicing regulation by TDP-43. *Nat Neurosci* 14:452–458.
23. Wang Z, et al. (2010) iCLIP predicts the dual splicing effects of TIA-RNA interactions. *PLoS Biol* 8:e1000530.
24. Briese M, et al. (2016) Whole transcriptome profiling reveals the RNA content of motor axons. *Nucleic Acids Res* 44:e33.
25. Offen D, et al. (2009) Spinal cord mRNA profile in patients with ALS: comparison with transgenic mice expressing the human SOD-1 mutant. *J Mol Neurosci* 38:85–93.
26. Haasdijk ED, Vlug A, Mulder MT, Jaarsma D (2002) Increased apolipoprotein E expression correlates with the onset of neuronal degeneration in the spinal cord of G93A-SOD1 mice. *Neurosci Lett* 335:29–33.
27. Yan Y, Yang J, Bian W, Jing N (2001) Mouse nestin protein localizes in growth cones of P19 neurons and cerebellar granule cells. *Neurosci Lett* 302:89–92.
28. Morita T, Mayanagi T, Sobue K (2012) Caldesmon regulates axon extension through interaction with myosin II. *J Biol Chem* 287:3349–3356.
29. Oprea GE, et al. (2008) Plastin 3 is a protective modifier of autosomal recessive spinal muscular atrophy. *Science* 320:524–527.
30. Wagnon JL, et al. (2012) CELF4 regulates translation and local abundance of a vast set of mRNAs, including genes associated with regulation of synaptic function. *PLoS Genet* 8:e1003067.
31. Krueger BJ, et al. (2008) LARP7 is a stable component of the 7SK snRNP while P-TEFb, HEXIM1 and hnRNP A1 are reversibly associated. *Nucleic Acids Res* 36:2219–2229.
32. Egloff S, Van Herreweghe E, Kiss T (2006) Regulation of polymerase II transcription by 7SK snRNA: two distinct RNA elements direct P-TEFb and HEXIM1 binding. *Mol Cell Biol* 26:630–642.
33. Liu P, et al. (2014) Release of positive transcription elongation factor b (P-TEFb) from 7SK small nuclear ribonucleoprotein (snRNP) activates hexamethylene bisacetamide-inducible protein (HEXIM1) transcription. *J Biol Chem* 289:9918–9925.
34. Mita S, et al. (2015) Transcallosal projections require glycoprotein M6-dependent neurite growth and guidance. *Cereb Cortex* 25:4111–4125.
35. Tesseur I, et al. (2000) Expression of human apolipoprotein E4 in neurons causes hyperphosphorylation of protein tau in the brains of transgenic mice. *Am J Pathol* 156:951–964.
36. Tesseur I, et al. (2000) Prominent axonopathy and disruption of axonal transport in transgenic mice expressing human apolipoprotein E4 in neurons of brain and spinal cord. *Am J Pathol* 157:1495–1510.
37. Werner H, Dimou L, Klugmann M, Pfeiffer S, Nave KA (2001) Multiple splice isoforms of proteolipid M6B in neurons and oligodendrocytes. *Mol Cell Neurosci* 18:593–605.
38. Verheijen MH, et al. (2014) Increased axonal ribosome numbers is an early event in the pathogenesis of amyotrophic lateral sclerosis. *PLoS One* 9:e87255.
39. Kim TH, Leslie P, Zhang Y (2014) Ribosomal proteins as unrevealed caretakers for cellular stress and genomic instability. *Oncotarget* 5:860–871.
40. Wiese S, et al. (2010) Isolation and enrichment of embryonic mouse motoneurons from the lumbar spinal cord of individual mouse embryos. *Nat Protoc* 5:31–38.